HHS Public Access

Author manuscript

Biosens Bioelectron. Author manuscript; available in PMC 2022 January 01.

Published in final edited form as:

Biosens Bioelectron. 2021 January 01; 171: 112681. doi:10.1016/j.bios.2020.112681.

Detecting Cancer Metastasis and Accompanying Protein Biomarkers at Single Cell Levels using a 3D-Printed Microfluidic Immunoarray

Mohamed Sharafeldin[a,1], **Tianqi Chen**[a,1], **Gulsum Ucak Ozkaya**[b], **Dharamainder Choudhary**[c], **Alfredo A. Molinolo**[d], **J. Silvio Gutkind**[e], **James F. Rusling**[*,a,c,f,g,h]

[a]Department of Chemistry, University of Connecticut, Storrs, CT 06269, USA. [b]Department of Food Engineering, Chemical and Metallurgical Engineering Faculty, Yildiz Technical University, Istanbul, Turkey, 34210. [c]Department of Surgery, UConn Health, Farmington, CT 06032. [d]Department of Pathology and Moores Cancer Center, Univ. of Calif. San Diego, La Jolla, CA 92093-0012. [e]Department of Pharmacology and Moores Cancer Center, Univ. Calif. San Diego, UC San Diego, La Jolla, CA 92093-0012. [f]Institute of Material Science, Storrs, CT 06269, USA. [g]School of Chemistry, National University of Ireland at Galway, Ireland. [h]Neag Cancer Center, UConn Health, Farmington, CT 06032

Abstract

A low-cost microfluidic microarray capable of lysing cells and quantifying proteins released after lysis was designed and 3D-printed. The array lyses cells on-chip in lysis buffer augmented with a 2s pulse of a sonic cell disruptor. Detection of desmoglein 3 (DSG3), a metastatic biomarker for head and neck squamous cell carcinoma (HNSCC), along with two accompanying HNSCC biomarkers from a single cell lysate of oral cancer cell cultures was demonstrated. A lysis chamber and reagent compartments deliver reagents into detection chambers decorated with capture antibodies immobilized onto inner walls coated with a highly swollen 3D chitosan hydrogel film. Sandwich immunoassays are achieved when captured analytes labeled with biotinylated secondary antibodies, which then capture streptavidin-poly[horse radish peroxidase] (Poly-HRP). Subsequent delivery of super-bright femto-luminol with H_2O_2 generates chemiluminescence captured with a CCD camera. DSG3 is membrane-bound protein in HNSCC cells of invaded lymph nodes, vascular endothelial growth factor-A (VEGF-A), vascular endothelial growth factor-C (VEGF-C) were positive controls overexpressed into the HNSCC culture medium. Beta-tubulin (β-Tub) was

[*]**Corresponding author:** james.rusling@uconn.edu.

[1]These Authors contributed equally to the manuscript

CRediT authorship contribution statement.

Mohamed Sharafeldin: Conceptualization, Investigation, Writing and editing the draft. **Tianqi Chen:** 3D design, Investigation, Writing and editing the draft. **Gulsum UCAK OZKAYA:** Investigation. **Dharamainder Choudhary:** Growing cell culture samples. **Alfredo A. Molinolo:** Methodology, conceptualization. **J. Silvio Gutkind:** Methodology, conceptualization, providing cell lines. **James F. Rusling:** Conceptualization, Supervision, reviewing and editing the draft.

The authors declare no competing financial interests.

used as a loading control to estimate the number of cells in analyzed samples. Limits of detection (LOD) were 0.10 fg/mL for DSG3, and 0.20 fg/mL for VEGF-A, VEGF-C and β-Tub. Three orders of magnitude semilogarithmic dynamic ranges were achieved. VEGF-A showed high in-cell expression, but VEGF-C had low levels inside cells. The very low LODs enabled quantifying these proteins released from single cells. Strong correlation between results from on-chip cell lysis, conventional off-line lysis and ELISA confirmed accuracy.

Graphical Abstract

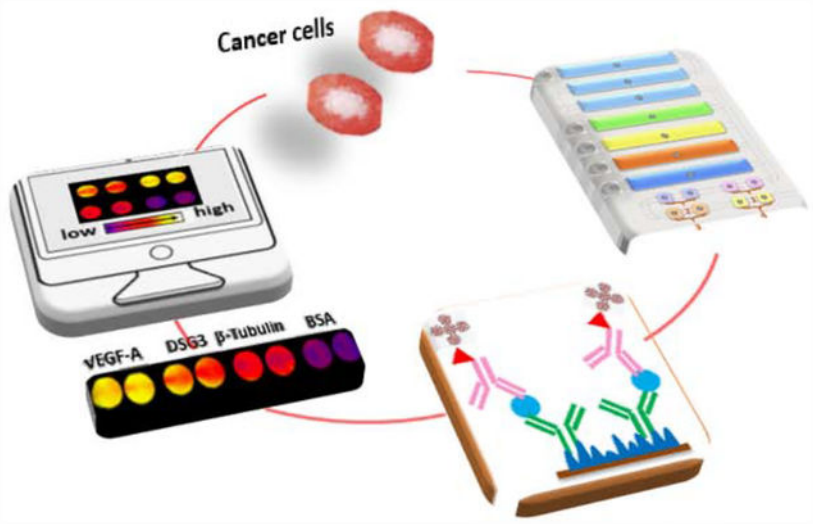

A 3D printed microfluidic array with on-line cell lysis was developed for single cell assays to detect metastatic cancer biomarker proteins at sub-fg/mL levels

Keywords

Chemiluminescence; Microfluidics; HNSCC; Metastatic Cancer Biomarkers; Single cell; 3D Printing

INTRODUCTION

Ninety percent of all cancer deaths are caused by metastasis of original tumors (Spano et al., 2012), and early detection leads to improved survival of cancer (Kalinich and Haber, 2018) and cancer metastasis patients (Gerges et al., 2010). While the approach reported here is applicable to any cancer and virtually any type of cells, the main goal of this work is to demonstrate the ability to quantify ultralow concentration of desmoglein 3 (DSG3) as a membrane-bound diagnostic biomarker for lymph node metastasis in oral cancer, or head and neck squamous cell carcinoma (HNSCC) (Siriwardena et al., 2018; Apu, et al., 2018). Membrane protein DSG3 is a biomarker for occult lymph node metastasis of HNSCC (Patel et al., 2013). It is highly expressed in metastatic oral cancer cells in neck lymph nodes, but not found in non-invaded lymph nodes (Patel et al., 2008). Oral cancer has an unusually high tendency to metastasize due to an extensive nearby neck lymphatic network (Leemans et al., 1994; Forastiere et al., 2001; Marur and Forastiere, 2016; De Zinis et al., 2006). Incidence of

occult lymph node metastasis ranges between 10 – 50% (Shah et al., 1990; Kuriakose and Trivedi, 2009; Mücke et al., 2014; Read on NIH website on head and neck cancer, 2020; Read online on Genetics Home Reference, 2020; Koloutsos et al. 2014; Dogan et al., 2014). Thus, rapid and sensitive diagnosis of lymph node metastasis is essential for HNSCC prognosis and key for clinical staging and treatment decisions (Kuriakose and Trivedi, 2009; Snow et al., 1982).

The histopathological hematoxylin-eosin (H&E)-immunohistochemistry (IHC) assay (de Bondt et al., 2007; Alkureishi et al., 2009; Don et al., 1995) can detect metastatic lesions ~0.2 mm in lymph nodes, but requires days to deliver the report and cannot be used for in-operative staging. Modern imaging tools (Di Gioia et al., 2015; de Bree et al., 2014; Chaturvedi et al., 2015), and assays of circulating cancer cells (Gerges et al., 2010) are not yet sensitive enough to detect very early metastasis. Real time (RT)-PCR, single-cell RNA sequencing and other next generation sequencing techniques can detect metastasis at single cell level coupled with robust cell sorting techniques such as fluorescence-activated cell sorting (FACS), but are relatively expensive, require long assay time and technical skills, and are mostly available in the research setting to date (Ferris et al., 2011; Ellsworth et al., 2017). H&E- IHC of sentinel lymph nodes remains the preferred option, despite false negatives due to failure to detect lesions <0.2 mm (Ferris et al., 2011; Kim et al., 2013). Thus, there is urgent need for fast, accurate, and ultrasensitive in-operative detection of metastatic oral and other cancers.

Microfluidics can be used to design fast, reliable platforms for ultrasensitive automated multi-protein assays (Rusling, 2013). Microfluidic tools possess inherent qualification for low-cost production, ease of complex fluid handling, miniaturization and automation (Whitesides, 2006). With high surface area to volume ratio, microfluidics allowed ultrasensitive detection of analytes from small volumes due to improved interaction kinetics between targets and surface biorecognition elements. This interaction allows development of assays with much shorter assay time and lower cost compared to other protein quantification techniques (Sackmann et al, 2014; Sia et al, 2008; Henares et al, 2008). We previously demonstrated the use of an amperometric microfluidic immunosensor to detect low concentrations of DSG3 as a reliable oral cancer biomarker for lymph node metastasis (Patel et al., 2013). Several microfluidic immunosensors using electrochemical, fluorescent, electrochemiluminescent (ECL), and chemiluminescent (CL) detection have been developed to measure multiple protein and peptide biomarkers for cancer diagnostics (Malhotra et al., 2012; Kelley et al., 2014; Dixit et al., 2016; Otieno et al., 2016; Tang et al., 2017). These devices have been integrated with different signal amplification approaches, such as nanoparticles or magnetic beads-HRP conjugates loaded with thousands of enzymes and antibodies in electrochemical and CL detection, antibody-coated Ru-$(bpy)_3^{2+}$-doped silica nanoparticles in ECL detection, immunohybridization chain reaction (HCR) in electrochemical and fluorescent detection. The assay sensitivity was mostly limited to 5–100 fg/mL, while Zhang (Zhang et al., 2012) reported a detection limit of 0.1 fg/mL using gold nanoparticle (NP)-assisted immuno-HCR. Although highly sensitive, HCR requires a cocktail of enzymes, DNA primers, and extensive optimizations to achieve such sensitivity and still suffers from nonspecific interactions between NPs and cell lysate components (Zhang et al., 2012; Bi et al., 2017). CL used for signal transduction needs no excitation

light, therefore minimizes background and is promising for lower detection limits compared to other optical methods like fluorescence. Recently emerged desktop 3D printers offer a revolutionary, low cost tool to rapidly develop and fabricate high performance microfluidic sensor arrays (Kadimisetty et al., 2018; Rusling, 2018; Sharafeldin et al., 2018). Chemical and ultrasonic cell lysis for the extraction of intracellular proteins have been well studied (Shehadul Islam et al., 2017; Nan et al., 2014), and these results supported our endeavors toward an automated microfluidic-lysis immunoarray.

Detection of proteins at the single-cell level could provide unprecedented understanding of disease progression and holds the potential for development of novel diagnostic tools at very early stages of disease. Various approaches have been developed to separate target cells from a population of cells (cell sorting) followed by proteomic analysis. These include a DNA-encoded antibody library (DEAL) to develop a single-cell barcode chip assay (Ma et al., 2011), used to detect proteins secreted form intact single cells sequestered within a PDMS trap (Lu et al., 2015). DEAL was also used to quantify secreted proteins from cells lysed on-chip, but with limited sensitivity (low pg/mL limits of detection, LOD) (Shi et al., 2012). Other DNA-based antibody coding was used for multiplexed screening of cell-surface proteins (Stoeckius et al., 2017; Peterson et al., 2017). While DNA-encoding provide a powerful multiplexing tool, it requires extensive engineering and optimization to overcome cross-talk and nonspecific interactions between nucleotides, proteins and antibodies. Alternatively, single phenotypes of cells were sorted using fluorescence-assisted cell sorting (FACS) combined with mass spectrometry (MS) to screen proteins, but this approach had limited sensitivity and high costs (Chen et al., 2019). Other single cell protein analysis technologies include micro-engraving, droplet microfluidics, single cell western blot, and magnetic ranking cytometry. All these techniques, though promising, have not achieved high detection sensitivity, multiplexing capabilities, or high cost (Labib and Kelley, 2020).

In this paper, we describe a 3D printed microfluidic array for ultrasensitive CL detection of proteins at single cell levels. Intact cell samples are introduced into the device and lysed by sonic-assisted chemical lysis. Detection chambers are coated with a chitosan hydrogel film that swells into a 3D structure with immobilized capture antibodies (Fig. 1). This open-network 3D hydrogel structure helps increase antibody surface coverage and availability, which in combination with poly-HRP labels and ultrabright femto-luminol for CL generation, provided ultra-high assay sensitivity (LOD <1 fg/mL), and good correlation with enzyme linked immunosorbent assays (ELISA). The new immunoarray-lysis device has LODs 10,000-fold better than the best reported ELISA LODs of several pg/mL (Jones et al., 2020; Zhang et al., 2014), and 1000-fold better than reported lateral flow assay (LFA) of sub pg/mL (Wu et al., 2013; Li et al., 2020). While some lateral flow assays achieve protein multiplexing, they do not support multifunctionality with integrated sample treatments like lysis and often suffer from low reproducibility (D. Bishop et al., 2019).

We report here the first immunoarray, to our knowledge, that determines proteins released from a single cell with online cell lysis and multiplexed protein detection without the need for pre-analysis cell sorting. The device provides the ability to quantify an intracellular, phenotype-specific protein, DSG3, at ultralow concentration (0.1 fg/mL). Quantifying soluble proteins like VEGF-A and VEGF-C as positive controls for HNSCC was used to

determine sample type (Fountzilas et al., 2006), HNSCC positive or negative, and limit false positive results. Automated assay in < 1 hr and very low cost (~$6/assay), are major advantages of this technique. This strategy was able to detect DSG3 at the single cell level with limit of detection (LOD) 0.10 fg/mL and 0.25 CL units (CLU)/log(fg/mL) sensitivity. VEGF-A had LOD 0.20 fg/mL and sensitivity of 0.31 CLU/log (fg/mL), VEGF-C had LOD 0.20 fg/mL and sensitivity of 0.08 CLU/log(fg/mL) and β-Tub had a 0.20 fg/mL LOD and 0.05 CLU/log (fg/mL).

RESULTS

Microfluidic chip design.

A five-inlet disposable microfluidic chip design isolated reagents and samples before detection was fabricated with a Form 2 3D stereolithographic printer from Formlabs polyacrylate Clear Resin (F2-GPCL-04) at a cost of ~ $0.60 (Fig S5, SI). Five 80 μL chambers were prefilled with sample, and solutions of biotinylated antibodies, poly-HRP, CL reagent and wash buffer (PBS-T20) (Fig. 1). Sample and reagent chambers sequentially fed a detection compartment featuring 8 detection chambers (8 μL ea.) filled with chitosan hydrogel and attached capture antibodies to measure 3 protein biomarkers and bovine serum albumin (BSA) as negative control in duplicates. Programmable peristaltic micropumps (Takasago Fluidic Systems) delivers sample and reagents to the chambers with flow controlled by an Arduino® microcontroller (Fig. 1). Micropumps are housed in a 3D printed support accommodating a sonic cell lysis probe (Sonic Soak) directly under the sample chamber. Detailed information of assay preparations and procedures can be found in Video S1, SI. Total cost of hardware is ~$330. A single assay costs ~ $6 in consumables.

Chitosan film characterization.

The 3D chitosan film strongly physiosorbed on inner walls of the individual detection chambers offers a highly porous hydrogel for anchoring massive numbers of capture antibodies (Ab_1). White light interferometry images shows large peaks (5–33 μm high) and ~10% valleys (Fig. 2 A, B). The chitosan film after swelling contains water at ~600% × total mass (Sharafeldin et al., 2019), and volume of the wet film increased 1000% compared to a dry film (Fig 2, C–F). These huge volume and mass increments along with rough surface allowed immobilization of ~1.0×10^{13} antibodies/cm^2 in the detection chambers (Table S1, SI).

Multiplexed protein assay.

Detection antibody (Ab_2) and polyHRP concentrations and incubation times required to capture target proteins from lysates by Ab_1 in detection compartments were optimized for highest signal to noise ratio and highest analytical sensitivity (Fig S1–S4, SI). The optimized protocol was used to quantify selected proteins. Standards were prepared in RIPA lysis buffer (50 mM Tris-HCl, pH 8.0, with 150 mM sodium chloride, 1.0% Igepal CA-630 (NP-40), 0.5% sodium deoxycholate, and 0.1% sodium dodecyl sulfate, and 2% Halt Protease and Phosphatase Inhibitor Single-Use Cocktail) spiked with 5x diluted human serum as a surrogate for a complex protein matrix. Fig 3 shows calibration curves for the biomarker proteins with standard deviations less than 20% at each concentration. Fig. 3A

and 3B show re-colorized CL images captured from analysis of standard protein surrogates and cell culture analysis. The BSA negative control was used to normalize the measured signals for target proteins and showed, along with the non-spiked control surrogates, a consistent very low background. This demonstrated that non-specific adsorption had a limited contribution to the measured signal, and if any, it was neutralized by the normalization against BSA negative controls. Limit of detections (LOD) were 0.10 fg/mL for DSG3, 0.20 fg/mL for VEGF-C, 0.20 fg/mL for VEGF-A, and 0.20 fg/mL for β-Tub. Dynamic ranges were 0.10–100 fg/mL for DSG3, 0.20–200 fg/mL for VEGF-C, 0.20–120 fg/mL for VEGF-A and 0.20–100 fg/mL for β-Tub. The ability to detect sub-fg levels of DSG3, VEGF-A and VEGF-C promised single cell analyses. β-Tub, a loading control in western blots (Liu and Xu, 2006; Li and Shen, 2013), was measured as a cell counting marker for highly diluted samples.

DSG3 has expression levels of 90–250 fg/tumor cell which is well above the assay LOD. VEGF-C and VEGF-A are positive protein biomarkers inside cells and expressed into the culture media as well. VEGF-C in the cell culture media has levels higher than 100 pg/mL which fits assay dynamic range after dilution. VEGF-C was undetectable in washed cells without culture media, while VEGF-A was detected in both washed cells and in culture media.

Effect of Sonication.

To test the effect of sonication on lysis efficiency, lysis in the chip was done with lysis buffer only with no sonication, and compared to lysis with buffer augmented with either 2s or10s sonic pulse. Lysis was also tested in PBS buffer (no lysis buffer) with 0, 2 and 10s sonication. With no sonication, lysis buffer and PBS buffer samples had concentration of VEGF-C 10±5 pg/mL and DSG3 and β-Tub were undetectable. With 2s sonication in lysis buffer, DSG3 and β-Tub were found at 50–150 fg/mL with 11±3 pg/mL VEGF-C. PBS buffer with 2s sonication also gave levels of DSG3 and β-Tub (2–10 fg/mL) but at lower concentrations compared to experiments using only lysis buffer. With 10s sonication in lysis buffer there was no noticeable change in found protein concentration compared to 2s sonication, but 10s sonication in PBS buffer showed increased DSG3 and β-Tub (Fig 4). Results underline the need for a sonic pulse in lysis buffer to release target membrane proteins.

Assay validation.

Selected concentrations of analyte proteins in RIPA buffer + 5% human serum to as surrogate for a complex protein matrix were determined on the same day using different chips to estimate intra-day variation. Relative standard deviations (RSD) were 11% for DSG3, 9% for VEGF-C and 14% for β-Tub. Similarly, inter-day variations over five days were RSD 13% for DSG3, 12% for VEGF-C and 17% for β-Tub. Recoveries from spiked protein cell lysates after subtracting control signals were between 80% and 120%, indicating analytically acceptable accuracy (Shah et al., 2000) (Table S2, SI).

Comparison of online and offline lysis.

Four cell lines were used to assess performance of the assay to lyse cells online and quantify proteins in the lysates. HN12, HN13, HN30 and Cal27 oral cancer cell line samples were also lysed offline using a previously reported procedure (Patel et al., 2013), and target analytes were quantified using the microfluidic chip. Culture media were diluted 10^4-times to 100 cell/mL, and 80 μL of samples containing cells from each cell line were analyzed. Strong correlation between results obtained from on-line and off-line lysis demonstrated the efficiency of the on-line cell lysis protocol (Fig 5). Also, cell samples were lysed using offline lysis and target protein biomarkers were quantified in lysates using ELISA. Good correlation between ELISA and our microfluidic lysis chip assay confirmed accuracy (Fig. 5). One-way ANOVA was used to compare the results of the three analytical techniques for target proteins in each of the analyzed cell lines. Results showed no statistical difference between online cell lysis or offline cell lysis with CL microfluidic protein detection, or offline cell lysis combined with ELISA (P-value > 0.05) (Table S3, SI). The amount of β-Tub per cell for each cell line was estimated by dividing the found β-Tub concentration by the counted number of lysed cells (100 cell/mL) in each sample based on the data from Fig 5 for later use as a cell counter.

Single Cell Protein Measurements—Individual cell separation was not done in this study, but highly diluted samples from cell cultures were tested. Samples were diluted until approximately a single cell remained (cell cultures were diluted 10^6-times). 10 μL of diluted samples were loaded into the sample chamber, and analyzed using online lysis. Due to cell-to cell variations (heterogenicity) and absence of cells in some diluted samples, trials from the same cell line can end up finding no cells or one single cell, as labeled on the bar in Fig. 6. Using the previously obtained protein calibration curves, β-Tubulin content per single cell was estimated for each cell line using samples in which the cells had been pre-counted. That is, numbers of cells in the highly diluted samples were estimated from β-Tub concentration divided by average β-Tub conc./cell, to find if specific analyzed samples contained single cell nor no cell. Then, assay response was related to protein levels of DSG3, VEGF-C and VEGF-A plotted on the graphs (Fig 6). Fig. 6 (A–D) shows protein concentrations found in diluted samples, without washing the cells to remove culture medium, and thus represents intracellular components and soluble proteins secreted into the culture medium. We found high levels of VEGF-C in all samples due to its solubility and expression into the cell culture media, noted as “Cell+Media” on the bars of Fig 6 (A–D). Thus, VEGF-C can be detected even though no cells were introduced into the chip for analysis. We then measured VEGF-C without the culture medium in isolated cells washed three times with osmotically balanced PBS. Fig. 6 (G–H) demonstrates found protein concentrations in culture medium-free cells, after washing cells and suspending them in PBS, thus represent intracellular protein expression. VEGF-C was not detected in any washed cells from any of the tested cell lines. VEGF-A was found in washed cells at detectable levels qualifying it to be a good control biomarker for oral cancer cells. Washed cells were then diluted in PBS buffer to single cell content (10 μL) and analyzed for VEGF-A, DSG3, and β-Tub with BSA as negative control. Fig. 6 (G–H) shows DSG3 and VEGF-A levels in single cells where number of cells were estimated using the β-Tub concentration as previously described. VEGF-A was detected in washed cells and had good correlation to DSG3 in the analyzed cell samples.

DISCUSSION

We described above a microfluidic device for online cell lysis coupled to ultrasensitive detection of a panel of 4 proteins with the ability to quantitatively detect a membrane-bound metastasis biomarker protein for oral cancer and associated soluble protein biomarkers at the single cell level. This is the first microfluidic device with sub-fg level sensitivity for single cell protein measurements and cancer metastasis to our knowledge. Cell lysis employs RIPA chemical lysis augmented by a 2s pulse of a 50 KHz sonic wave. Ultrasonication was essential for cell lysis, and also helps mix cells with RIPA lysis buffer in the sample chamber. This approach allowed fully automated system operation, eliminating the need to manually mix cell samples with lysis buffer before the assay.

The protein biomarker panel used allowed us to fully develop an assay relevant to membrane bound cancer metastasis biomarkers. DSG3 is exclusively expressed in oral cancer cells invaded into lymph nodes, absent in non-invaded lymph nodes, and not expressed into blood or lymphatic fluid (Patel et al., 2013). The ability to detect sub-femtogram levels of DSG3 enabled detection of a single metastasized cell. VEGF-A has also been previously reported to have strong correlation to state of head and neck cancer metastasis (Sousa et al., 2014; Zhang et al., 2015). Measuring VEGF-A and DSG3 in the same assay will increases significance of assay outcomes related to metastasis. The assay is also general, and adaptable to any small biomarker panel including membrane bound proteins, the number of proteins determined could be increased by increasing the number of detection wells in the 3D printed chip.

The use of chitosan hydrogel to immobilize antibodies provided a 3D platform for antibody-antigen interaction improving interaction kinetics which in turn was reflected in decreased assay time and increased sensitivity. The 30 trillion Ab_1 per well in this immunoarray is much larger than 0.36 trillion Ab_1 on a flat 0.012 cm^2 sensors, and 6 trillion on SWCNT forest arrays (Malhotra et al., 2010). Thus, Ab_1-loading in the present work is 5-fold greater than on our previous SWCNT arrays with 5 fg/mL LOD for DSG3 (Patel et al., 2013). The highly swollen chitosan hydrogel featuring water filled channels inside a 3D network facilitate mass transport of labeled analyte to find and bind to Ab_1 in the detection chambers. Improved interaction kinetics is also facilitated by the microfluidic detection compartment with low volume/surface area ratio (10 μL/cm^2). This helps accelerate mass transport-controlled analyte-antibody binding, decreasing assay time while maintaining ultra-sensitivity. The use of polymeric streptavidin multi-labelled with 400 HRP enzymes in poly-HRP combined with ultra-bright CL reagent femto-luminol provided large signal amplification, resulting in the sub femtogram LODs, and providing bright images even at very low analyte concentrations. CL images may appear inhomogeneous due to the change of the interaction kinetics between HRP/Luminol and enhancers over the course of image acquisition reported in many CL/ECL systems (Maus et al., 1999; Bi et al., 2013; Zong et al., 2014).

CONCLUSIONS

An ultra-sensitive detection device for proteins extracted from within single cells was developed and validated. The technique features the first sub-fg detection level microfluidic device with on-chip lysis and chemiluminescent detection for single cell protein measurement, and is applicable to cancer metastasis diagnostics. This system achieved sub-femtogram LODs of cell-residing proteins in a single cell, which was further enhanced by high signal amplification from streptavidin-Poly-HRP labels and ultrabright femto-luminol. Future work will adapt the immunoassay to real-time surgery room settings in which sectioned lymph node tissue can be introduced, lysed, and analyzed on a suitably modified chip. Additionally, on-chip single cell isolation will be designed and implemented, so that cancer cells can be separated from normal cells in tissue before lysis and detected without any pre-treatment.

MATERIALS AND METHODS

Materials.

All reagents and chemicals were of analytical grade. Chitosan (low molecular weight) and glutaraldehyde were from Sigma Aldrich. Blocker casein in PBS buffer was from Thermo Fisher. ELISA kit for Vascular Endothelial Growth Factor-C (VEGF-C) (DY752B), and Vascular Endothelial Growth Factor-A (VEGF-A) (DY293B) were from R&D Systems. Human Desmoglein3 (DSG3) monoclonal antibody (MAB1720), human DSG3 biotinylated polyclonal antibody (BAF1720), recombinant human DSG3 chimera protein (1720-DM) and bovine serum albumin (BSA) were purchased from R&D Systems. Monoclonal [EP1331Y] beta-Tubulin antibody, biotinylated monoclonal [BT7R] beta-Tubulin antibody and recombinant human beta-Tubulin protein (ab70187) were from Abcam®. RIPA lysis buffer (50 mM Tris-HCl, pH 8.0, with 150 mM sodium chloride, 1.0% Igepal CA-630 (NP-40), 0.5% sodium deoxycholate, and 0.1% sodium dodecyl sulfate, and 2% Halt Protease and Phosphatase Inhibitor Single-Use Cocktail) was from Sigma Aldrich. Chemiluminescence (CL) was generated using Thermo Fisher Supersignal® West Femto chemiluminescent substrate, containing femto-luminol and hydrogen peroxide mixed immediately before use. Streptavidin-Poly(Horseradish Peroxidase) (Poly-HRP80) conjugate was obtained from Fitzgerald®. CL was measured using a Syngene® dark box with CCD camera. Images were processed using GeneSnap® software. Phosphate buffer saline (PBS) pH 7.4 was 0.01 M sodium phosphate in 0.14 M NaCl and 2.7 mM KCl. Phosphate buffer saline-tween20 (PBS-T20) was 0.01 M sodium phosphate in 0.14 M NaCl, 2.7 mM KCl and 0.05% Tween-20. Oral cancer cell lines CAL27 was from ATCC (Va), HN12, HN13 and HN30 were provided by Dr. Silvio Gutkind, University of California San Diego, and cultured in Dulbecco's modified Eagle medium (DMEM) supplemented with 10% fetal bovine serum at 37°C in the presence of 5% CO_2 as described previously (Jeon et al., 2004).

Antibody immobilization.

Capture antibodies (Ab_1) were immobilized on the inner walls of each detection chamber using previously reported chitosan/glutaraldehyde chemistry (Sharafeldin et al., 2019). Briefly, a thin film of chitosan was formed on the inner walls of detection chambers by

adding 8 μL of 0.5 mg/mL chitosan in 0.05 M HCl (pH 4.0) into each detection chamber and was allowed to incubate for 3 hrs. Each detection chamber was equipped with a sample/reagent injection hole of 0.75 mm diameter, where antibody solutions were injected and removed. The hole was then blocked with a Kapton tape or a drop of PDMS to prevent leakage. After adding the tape, the hole maintained a tiny air bubble preventing the flowing samples and reagents from getting in direct contact with the adhesive layer. Chitosan solution was drained out and the liquid film was dried under vacuum at RT overnight. 8 μL of 3% glutaraldehyde in PBS (pH 8.0) was added to detection chambers for 3 hrs, washed with DI water and 8 μL of capture antibodies at pre-optimized concentrations were added and incubated overnight. Unbound antibodies were washed with PBS-T20 and detection compartments were incubated with 1% casein blocker buffer for 1 hr, washed with PBS-T20 and chips were stored at 4˚C until used. See Video S1, SI for more detailed information.

Multiplexed biomarker chemiluminescence assay.

80 μL of standards with different concentrations of biomarker panel prepared in RIPA buffer/5% human serum to mimic cell lysate surrogates were introduced into sample compartment through the injection hole as explained previously. Similarly, 80 μL of buffer, biotinylated antibodies, Poly-HRP, and luminescence substrate were introduced into their designated chambers through the injection hole that was blocked with Kapton tape afterwards (See Fig. 1 for chamber designation). Samples were delivered to detection compartment by activating sample pump for 25s at a flow rate of 200 μL/min, incubated for 20 min, and washed by activating the PBS-T20 pump for 1 min at a flow rate of 200 μL/min. Biotinylated detection antibodies (Ab_2) were delivered to detection compartment by activating Ab_2 pump for 30s at 200 μL/min, incubated for 15 min and washed with 200 μL PBS-T20 by activating PBS-T20 pump for 1 min. Poly-HRP was flowed to detection compartment by activating HRP pump for 30s, incubated for 10 min, and washed with 200 μL of PBS-T20. Finally, femto luminol chemiluminescence reagent was delivered to detection compartment and chemiluminescence signal was captured using a CCD camera for 15s. See Video S1, SI for more detailed information.

Assay Validation.

To assess the accuracy of assay, spiked concentration of each biomarker from protein depleted cell lysates was measured. The same chemiluminescent assay procedures were adopted to estimate the concertation of each protein biomarker.

Cell culture.

Cell cultures, HN12, HN13, HN30 and CAL27 were analyzed for the selected biomarker panel. Cells were cultured in DMEM supplemented with 10% fetal bovine serum (FBS) in presence of 5% CO_2 at 37°C. Cells with culture medium were collected by mechanical separation of adherent cell layer from culture plates and number of cells per mL were estimated by using manual cell counting.

Biomarker quantification from offline cell lysates.

Offline cell lysis was used as standard method to prepare cell lysates that was introduced directly into the sample chamber and delivered right away to detection compartment. Cells were lysed by incubation with RIPA lysis buffer for 20 min with intermittent vortexing. Cell lysates originally estimated to have 1×10^6 cells/mL were diluted 10^4X before introducing 80 μL of lysate (~ content of 100 cells/mL) into the sample chamber in order to bring biomarkers into the working concentration of the assay. Same chemiluminescent assay procedures were followed.

Biomarker quantification after online cell lysis.

Collected cells with culture medium was diluted 10^3 times and 5 μL of the dilute cell solution was introduced into the sample chamber containing 75 μL of RIPA lysis buffer (in total 10^4X dilution to ~ 100 cells/mL analyzed) through the sample injection hole. Once introduced, the ultrasonic probe (50 KHz) was activated for 2s to mix the cells with the lysis buffer and augmented the lysis process. Solution was kept in the sample chamber for 20 min, delivered to detection compartment and incubated for 20 min. Same chemiluminescent assay procedures were followed to quantify protein biomarkers.

Supplementary Material

Refer to Web version on PubMed Central for supplementary material.

ACKNOWLEDGEMENTS

The authors thank Taylor Jones, University of North Carolina at Charlotte, for help with 3D chitosan imaging. This work was supported financially by an Academic Plan Grant from The University of Connecticut and in part by Grant no. EB016707 from the National Institute of Biomedical Imaging and Bioengineering (NIBIB), NIH. The authors thank James F. Elman (Filmetrics Application Lab, Rochester, NY) for optical surface profiling.

REFERENCES

Alkureishi LWT, Burak Z, Alvarez JA, Ballinger J, Bilde A, Britten AJ, Calabrese L, Chiesa C, Chiti A, de Bree R, Gray HW, Hunter K, Kovacs AF, Lassmann M, Leemans CR, Mamelle G, McGurk M, Mortensen J, Poli T, Shoaib T, Sloan P, Sorensen JA, Stoeckli SJ, Thomsen JB, Trifiro G, Werner J, Ross GL, The European Association of Nuclear Medicine (EANM) Oncology Committee and European Sentinel Node Biopsy Trial (SENT) Committee, 2009 Eur J Nucl Med Mol Imaging. 36,1915–1936. [PubMed: 19784646]

Apu EH, Akram SU, Rissanen J, Wan H, Salo T, 2018 Exp. Cell Res 370, 353–364. [PubMed: 29969588]

Bi S, Ji B, Zhang Z, Zhang S, 2013 Chem. Commun 49, 3452–3454

Bi S, Yue S, Zhang S, 2017 Chem. Soc. Rev 46, 4281–4298. [PubMed: 28573275]

Chaturvedi P, Datta S, Arya S, Rangarajan V, Kane SV, Nair D, Nair S, Chaukar DA, Pai PS, Pantvaidya G, Deshmukh AD, Agrawal A, D'Cruz AK, 2015 Head Neck 37, 1504–1508. [PubMed: 24890924]

Chen C, Harst A, You W, Xu J, Ning K, Poetsch A, 2019 Biotechnology for biofuels 12, 21. [PubMed: 30740142]

Bishop D, J. V Hsieh H, Gasperino J, D. H Weigl B, 2019 Lab. Chip 19, 2486–2499. [PubMed: 31251312]

Don DM, Calcaterra TC, Anzai Y, Lufkin RB, Fu Y-S, 1995 The Laryngoscope 105, 669–674. [PubMed: 7603268]

De Zinis LOR, Bolzoni A, Piazza C, Nicolai P, 2006 Eur. Arch. Oto-Rhino-Laryngol. Head Neck 263, 1131–1135.

de Bondt RBJ, Nelemans PJ, Hofman PAM, Casselman JW, Kremer B, van Engelshoven JMA, Beets-Tan RGH, 2007 Eur. J. Radiol 64, 266–272. [PubMed: 17391885]

de Bree R, Takes RP, Castelijns JA, Medina JE, Stoeckli SJ, Mancuso AA, Hunt JL, Rodrigo JP, Triantafyllou A, Teymoortash A, Civantos FJ, Rinaldo A, Pitman KT, Hamoir M, Robbins KT, Silver CE, Hoekstra OS, Ferlito A, 2014 Head Neck 37, 1829–1839. [PubMed: 24954811]

de Sousa EA, Lourenço SV, de Moraes FPP, Vartanian JG, Gonçalves-Filho J, Kowalski LP, Soares FA, Coutinho–Camillo CM, 2014 Head Neck 37, 1410–1416. [PubMed: 24824527]

Dogan E, Cetinayak HO, Sarioglu S, Erdag TK, Ikiz AO, 2014 J. Laryngol. Otol 128, 268–273. [PubMed: 24548727]

Di Gioia D, Stieber P, Schmidt GP, Nagel D, Heinemann V, Baur-Melnyk A, 2015 Brit. J. Cancer 112, 809–818. [PubMed: 25647014]

Dixit CK, Kadimisetty K, Otieno BA, Tang C, Malla S, Krause CE, Rusling JF, 2016 Analyst 141, 536–547. [PubMed: 26525998]

Ellsworth DL, Blackburn HL, Shriver CD, Rabizadeh S, Soon-Shiong P, Ellsworth RE, 2017 Clin Trans Med 6, 15.

Forastiere A, Koch W, Trotti A, Sidransky D, 2001 N. Engl. J. Med 345,1890–1900. [PubMed: 11756581]

Fountzilas G, Angouridakis N, Wirtz RM, Claas S, Nikolaou A, Kalogeras KT, 2006 J. Clin. Oncol 24, 5538–5538.

Ferris RL, Xi L, Seethala RR, Chan J, Desai S, Hoch B, Gooding W, Godfrey TE, 2011 Clin Cancer Res. 17, 1858–1866. [PubMed: 21355082]

Genetics Home Reference Head and neck squamous cell carcinoma https://ghr.nlm.nih.gov/condition/head-and-neck-squamous-cell-carcinoma (last accessed May 22, 2020).

Gerges N, Rak J, Jabado N, 2010 British Med. Bull 94, 49–64.

Henares TG; Mizutani F; Hisamoto H, 2008 Anal. Chim. Acta 611, 17–30. [PubMed: 18298963]

Head and Neck Cancer Research https://www.cancer.gov/types/head-and-neck/research (last accessed May 22, 2020).

Jeon GA, Lee J-S, Patel V, Gutkind JS, Thorgeirsson SS, Kim EC, Chu I-S, Amornphimoltham P, Park MH, 2004 Int. J. Cancer 112, 249–258. [PubMed: 15352037]

Jones A, Dhanapala L, Kankanamage RNT, Kumar CV, Rusling JF, 2020 Anal.Chem 92, 345–362. [PubMed: 31726821]

Kuriakose MA, Trivedi NP, 2009 Curr. Opin. Otolaryngology & Head and Neck Surgery 17, 100–110.

Kim CH, Soslow RA, Park KJ, Barber EL, Khoury-Collado F, Barlin JN, Sonoda Y, Hensley ML, Barakat RR, Abu-Rustum NR, 2013 Int J Gynecol Cancer 23, 964–970. [PubMed: 23694985]

Kelley SO, Mirkin CA, Walt DR, Ismagilov RF, Toner M, Sargent EH, 2014 Nature Nanotech. 9, 969–980.

Koloutsos G, Vahtsevanos K, Kyrgidis A, Kechagias N, Triaridis S, Antoniades K, 2014 J. Craniofac. Surg 25, 1992–1997. [PubMed: 25329854]

Kadimisetty K, Malla S, Bhalerao KS, Mosa IM, Bhakta S, Lee NH, Rusling JF, 2018 Anal. Chem 90, 7569–7577. [PubMed: 29779368]

Kalinich M, Haber DA, 2018 Science 359, 866–867. [PubMed: 29472467]

Leemans CR, Tiwari R, Nauta JJP, Waal IVD, Snow GB, 1994 Cancer 73, 187–190. [PubMed: 8275423]

Li F, You M, Li S, Hu J, Liu C, Gong Y, Yang H, Xu F, 2020 Biotechnol. Adv 39, 107442. [PubMed: 31470046]

Liu N-K, Xu X-M, 2006 J. Neurotrauma 23, 1794–1801. [PubMed: 17184189]

Li R, Shen Y, 2013 Life Sci. 92, 747–751. [PubMed: 23454168]

Lu Y, Xue Q, Eisele MR, Sulistijo ES, Brower K, Han L, Amir ED, Pe'er D, Miller-Jensen K, Fan R, 2015 Proc. Natl Acad. Sci. USA 112, E607–E615. [PubMed: 25646488]

Labib M, Kelley SO, 2020 Nat Rev Chem 4, 143–158.

Maus RG, McDonald EM, Wightman RM., 1999, Anal. Chem 71, 4944–4950. [PubMed: 21662840]

Malhotra R, Papadimitrakopoulos F, Rusling JF, 2010 Langmuir 26, 15050–15056 [PubMed: 20731335]

Ma C, Fan R, Ahmad H, Shi Q, Comin-Anduix B, Chodon T, Koya RC, Liu C-C, Kwong GA, Radu CG, Ribas A, Heath JR, 2011 Nat Med 17, 738–743. [PubMed: 21602800]

Malhotra R, Patel V, Chikkaveeraiah BV, Munge BS, Cheong SC, Zain RB, Abraham MT, Dey DK, Gutkind JS, Rusling JF, 2012 Anal. Chem 84, 6249–6255. [PubMed: 22697359]

Mücke T, Mitchell DA, Wagenpfeil S, Ritschl LM, Wolff K-D, Kanatas A, 2014 BMC Cancer 14, 346–352. [PubMed: 24885244]

Marur S, Forastiere AA, 2016 Mayo Clin. Proc 91, 386–396. [PubMed: 26944243]

Nan L, Jiang Z, Wei X, 2014 Lab Chip 14, 1060–1073. [PubMed: 24480982]

Otieno BA, Krause CE, Jones AL, Kremer RB, Rusling JF, 2016 Anal. Chem 88, 9269–9275. [PubMed: 27558535]

Patel V, Hood BL, Molinolo AA, Lee NH, Conrads TP, Braisted JC, Krizman DB, Veenstra TD, Gutkind JS, 2008 Clin Cancer Res.14,1002–1014. [PubMed: 18281532]

Patel V, Martin D, Malhotra R, Marsh CA, Doçi CL, Veenstra TD, Nathan C-AO, Sinha UK, Singh B, Molinolo AA, Rusling JF, Gutkind JS, 2013 Oral Oncology 49, 93–101. [PubMed: 23010602]

Peterson VM, Zhang KX, Kumar N, Wong J, Li L, Wilson DC, Moore R, McClanahan TK, Sadekova S, Klappenbach JA, 2017 Nat Biotechnol 35, 936–939. [PubMed: 28854175]

Rusling JF, 2013 Anal. Chem 85, 5304–5310. [PubMed: 23635325]

Rusling JF, 2018 ACS Sens. 3, 522–526. [PubMed: 29490458]

Sackmann EK; Fulton AL; Beebe DJ, 2014 Nature 507, 181–189. [PubMed: 24622198]

Sia K, S. J Kricka L, 2008 Lab. Chip 8, 1982–1983. [PubMed: 19023459]

Snow GB, Annyas AA, van Slooten EA, Bartelink H, Hart AA, 1982 Clin Otolaryngol Allied Sci. 7, 185–192. [PubMed: 7105450]

Shah JP, Candela FC, Poddar AK, 1990 Cancer 66, 109–113. [PubMed: 2354399]

Shah VP, Midha KK, Findlay JWA, Hill HM, Hulse JD, McGilveray IJ, McKay G, Miller KJ, Patnaik RN, Powell ML, Tonelli A, Viswanathan CT, Yacobi A, 2000 Pharm. Res 17, 1551–1557. [PubMed: 11303967]

Shi Q, Qin L, Wei W, Geng F, Fan R, Shin YS, Guo D, Hood L, Mischel PS, Heath JR, 2012 Proc. Natl. Acad. Sci. USA 109, 419–424. [PubMed: 22203961]

Spano D, Heck C, Antonellis PD, Christofori G, Zollo M, 2012 Seminars in Cancer Biol 22, 234–249.

Shehadul Islam M, Aryasomayajula A, Selvaganapathy PR 2017 Micromachines 8, 83.

Stoeckius M, Hafemeister C, Stephenson W, Houck-Loomis B, Chattopadhyay PK, Swerdlow H, Satija R, Smibert P, 2017 Nat Methods 14, 865–868. [PubMed: 28759029]

Sharafeldin M, Jones A, Rusling JF, 2018 Micromachines 9, 394.

Siriwardena SBSM, Tsunematsu T, Qi G, Ishimaru N, Kudo Y, 2018 Int. J. Mol. Sci 19, 1462.

Sharafeldin M, Kadimisetty K, Bhalerao KR, Bist I, Jones A, Chen T, Lee NH, Rusling JF, 2019 Anal. Chem 91, 7394–7402. [PubMed: 31050399]

Tang CK, Vaze A, Rusling JF, 2017 Lab Chip 17, 484–489. [PubMed: 28067370]

Whitesides GM, 2007 Nature 442, 368

Wu Y, Xue P, Kang Y, Hui KM, 2013 Anal. Chem 85, 8661–8668. [PubMed: 23937646]

Zhang B, Liu B, Tang D, Niessner R, Chen G, Knopp D, 2012 Anal. Chem 84, 5392–5399. [PubMed: 22632712]

Zhang S, Garcia-D'Angeli A, Brennan JP, Huo Q, 2014 Analyst 139, 439–445. [PubMed: 24308031]

Zong C, Wu J, Liu M, Yang L, Yan F, Ju H, 2014 Anal. Chem 86, 9939–9944. [PubMed: 25181362]

Zhang B, Gao Z, Sun M, Li H, Fan H, Chen D, Zheng J, 2015 J. Surg. Oncol 111, 382–388. [PubMed: 25475162]

Highlights:

- This is the first automated 3D-printed microfluidic immunoarray capable of lysing by using a 50 KHz cell disruptor and quantifying released biomarker proteins bound to cells.
- Advantages over other single cell approaches are low cost, speed, accuracy and sensitivity.
- Unprecedented sub-fg/mL limits of detection are achieved by combining cylindrical detection chambers filled with capture antibodies on a highly swollen 3D chitosan hydrogel, streptavidin poly[horseradish peroxidase] (Poly-HRP) labels and ultrabright femto-luminol reagent to generate chemiluminescence
- Proteins residing within single cells were quantitatively measured

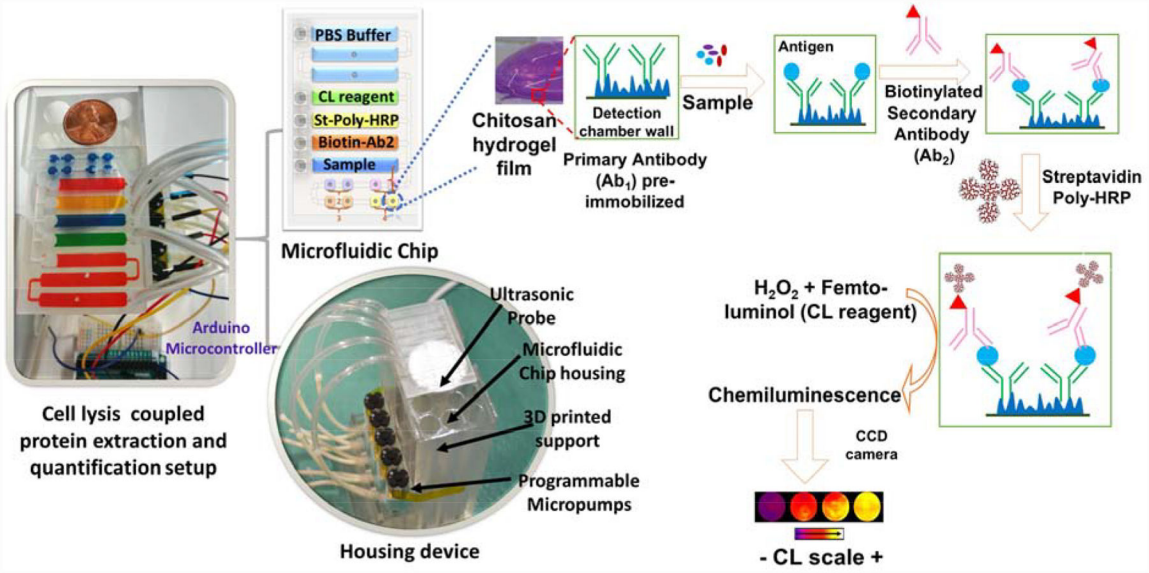

Fig 1.

Device design encompasses a microfluidic chip with 5 inlets connected to peristaltic micropumps, sample and rectangular prism reagent chambers with capacity of 80± 5 μL, and 8 cylindrical detection chambers with 8±1 μL capacity each; dimensions are 52 × 36 × 2.25mm (L×W×H). A microfluidic chip is designed to house sample and reagents and deliver them sequentially to detection compartment. The assay protocol utilizes poly-HRP and ultra-bright femto-luminol to produce chemiluminescence that is captured using a CCD camera. The microfluidic chip is mounted on the housing device support equipped with sonic lysis probe and micropumps. Programmable micropumps are connected to microfluidic chip sample and reagent chambers and controlled by an Arduino microcontroller.

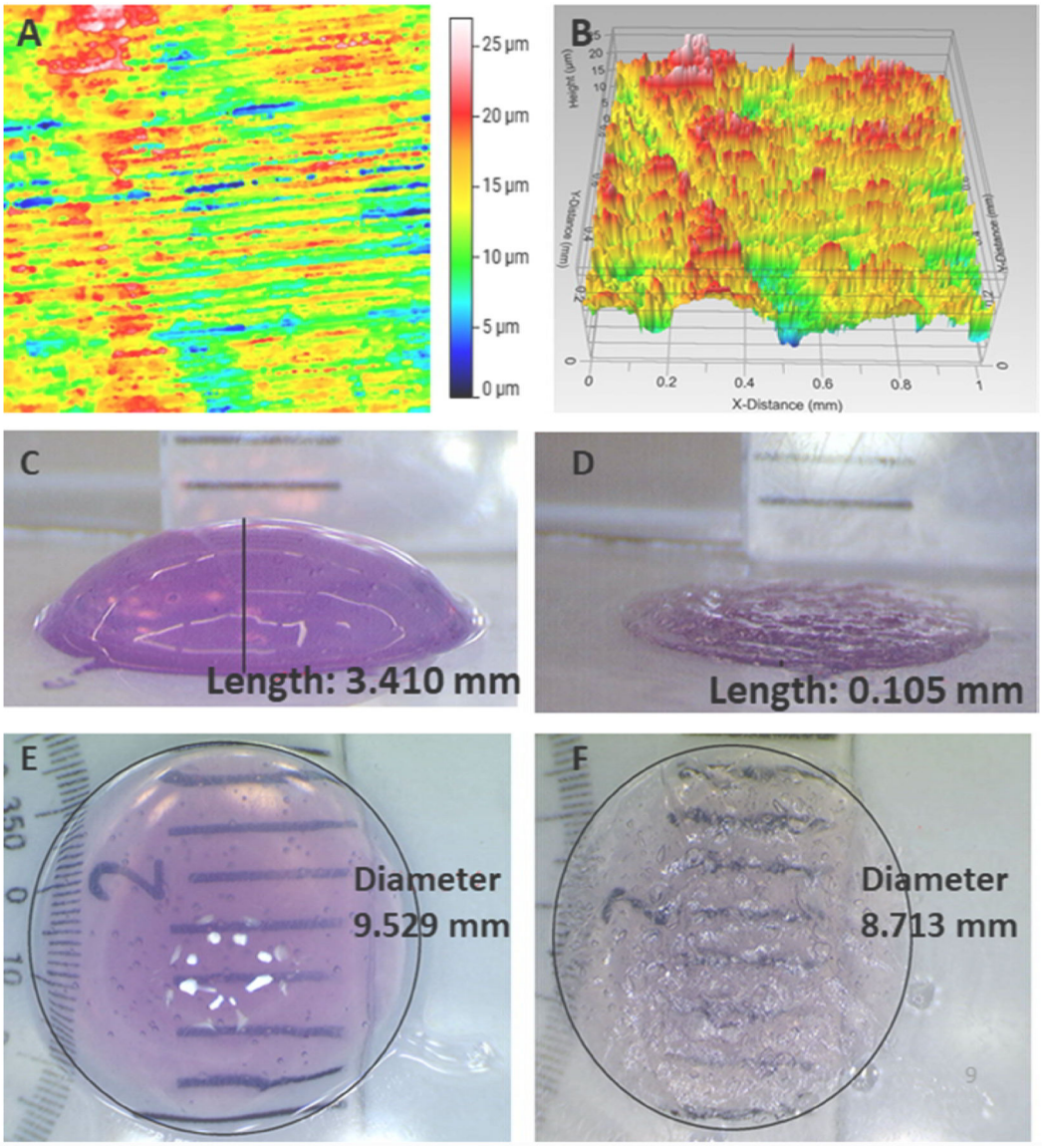

Fig. 2.

White light interferometry surface profile of chitosan-coated 3D printed polyacrylate surface: (A) top view and (B) side view. Digital microscope images of side view of a chitosan hydrogel hemisphere loaded with methylene blue dye (C) with water and (D) after drying. Digital microscope images of top view of chitosan hydrogel hemisphere loaded with methylene blue dye (E) with water and (F) after drying. Images show ~1000% increase in hemisphere volume after saturation with water.

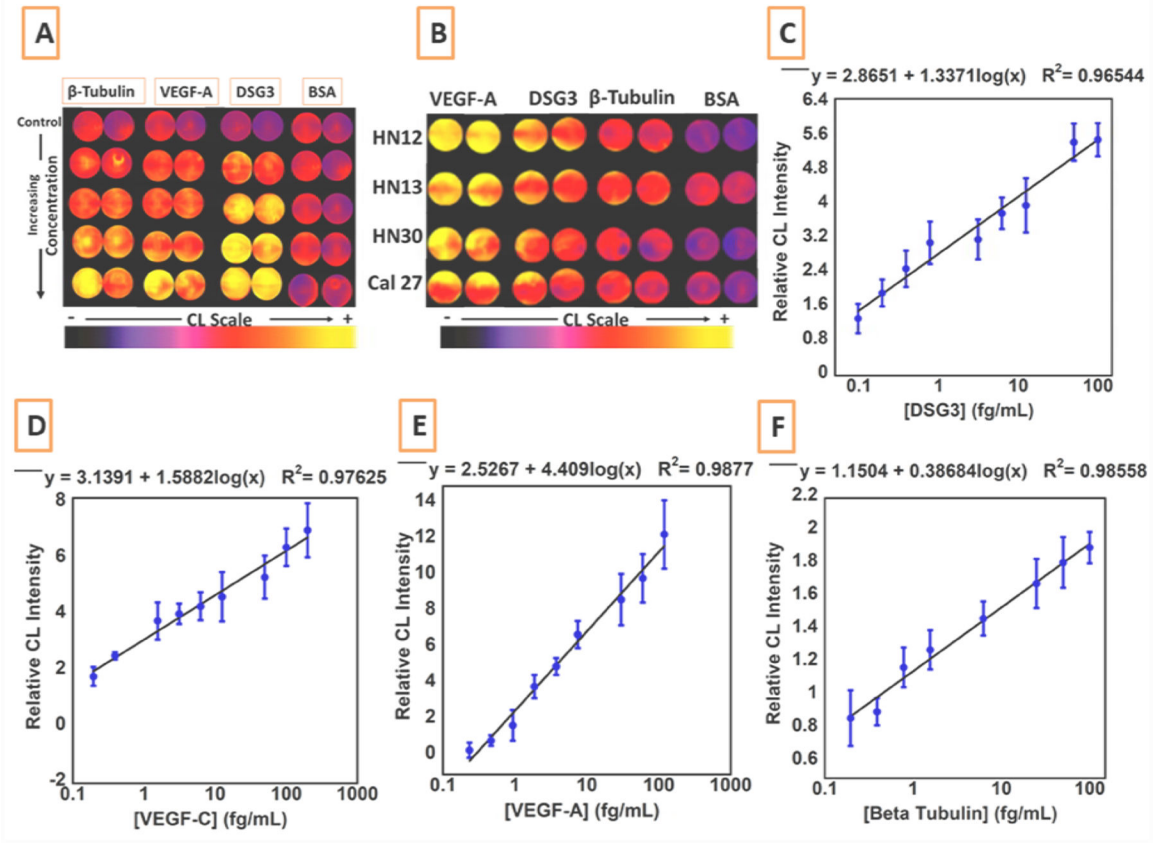

Fig 3.

Recolored CL images of (A) protein standards and (B) cell lines. Calibration curves obtained with the microfluidic microchip for (C) DSG3, (D) VEGF-C, (E) VEGF-A, and (F) β-Tub. CL signal was captured using CCD camera integration for 15 s. (n=8)

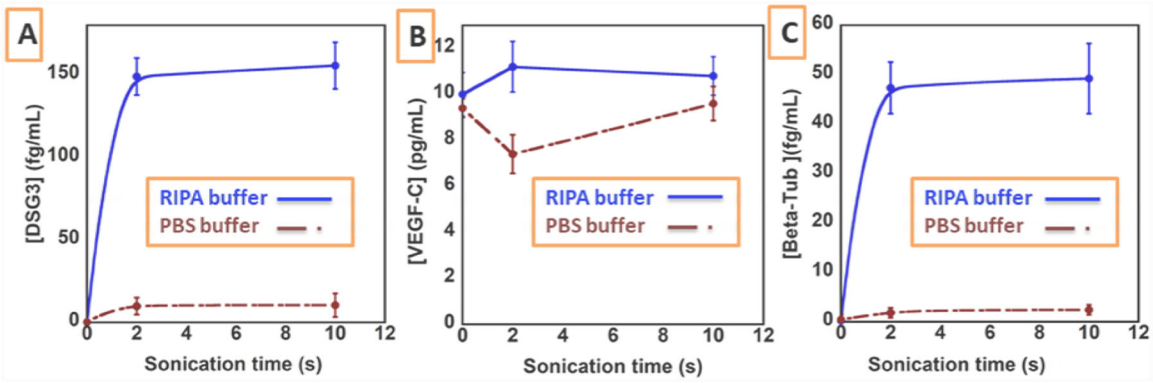

Fig 4.

Influence of sonic pulse time on the extraction and quantitation of (A) DSG3, (B) VEGF-C, and (C) β-Tub in RIPA lysis buffer (blue line) and PBS buffer (Red dotted line). Assay without sonication corresponds to data obtained at 0s sonication time. (n=4)

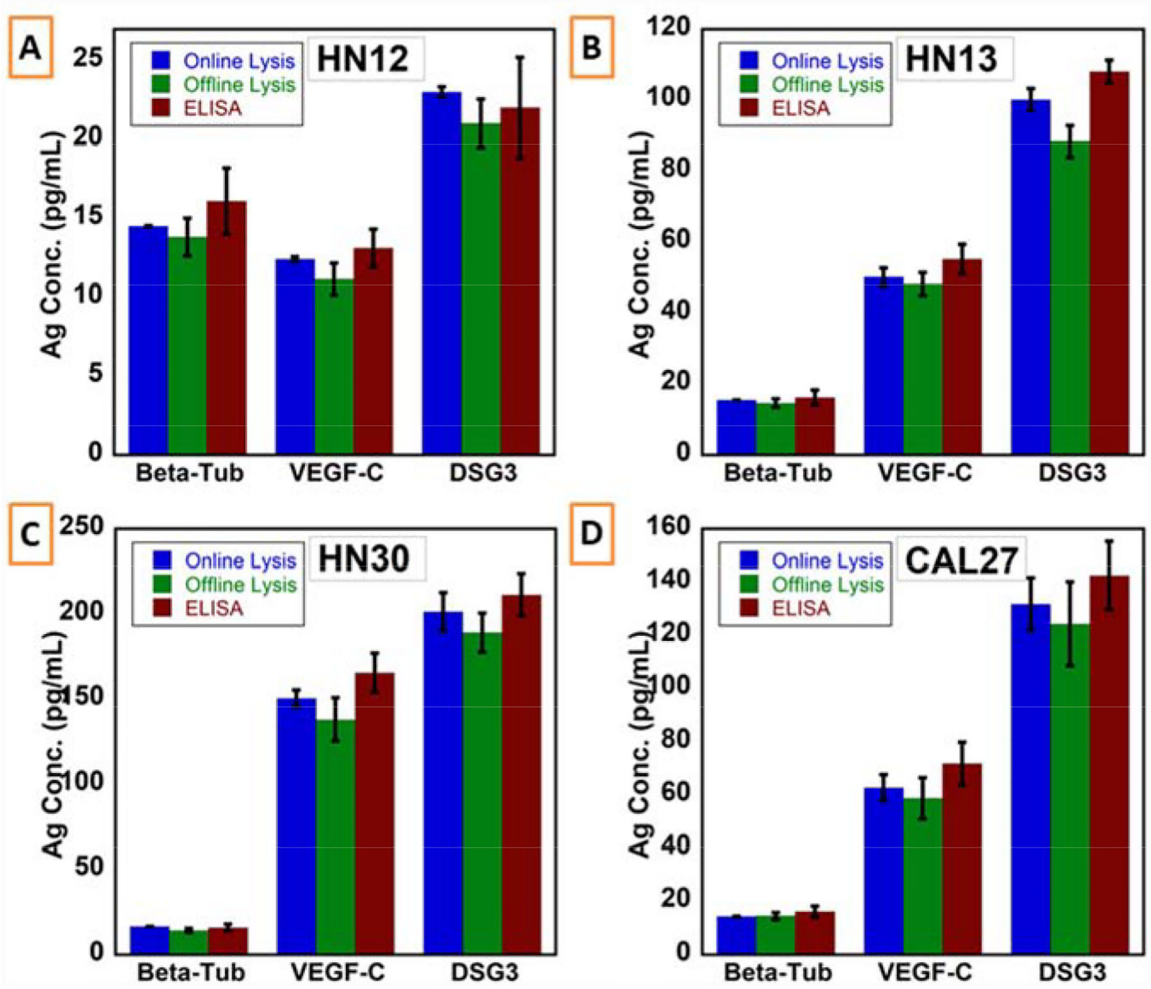

Fig 5.

Comparison of results obtained using online lysis, offline lysis and ELISA for cell lines (A) HN12, (B) HN13, (C) HN30 and (D) CAL27. (n=4)

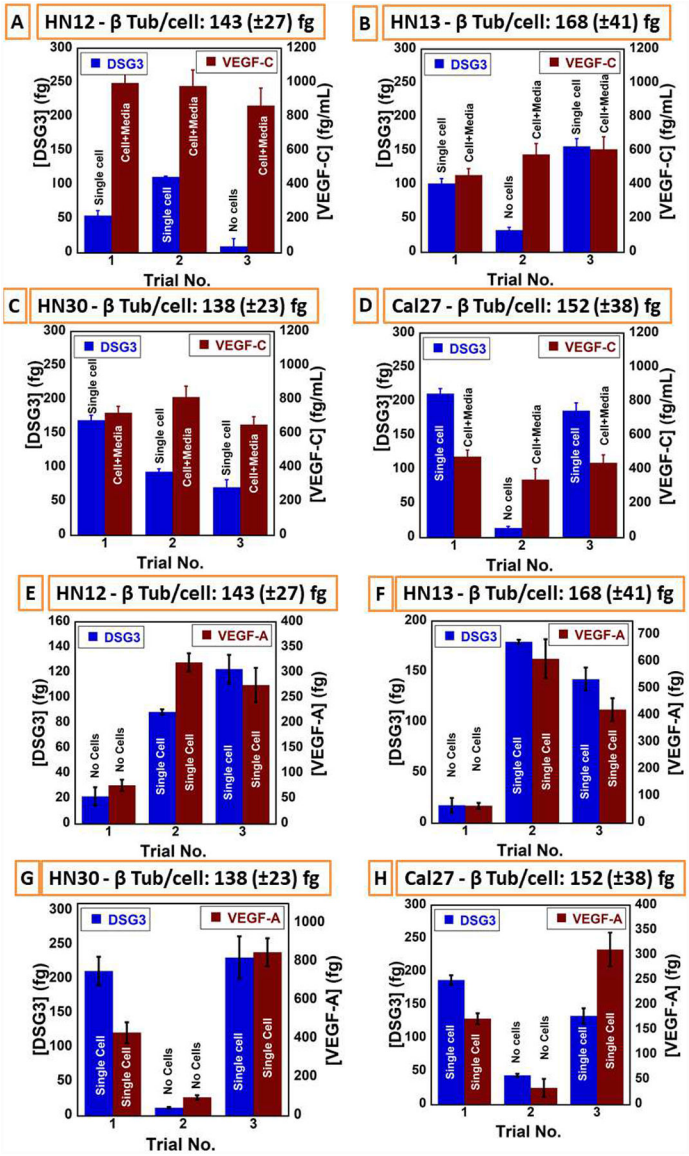

Fig 6.

Estimated biomarker concentration from single or no cell samples after online cell lysis including culture medium for (A) HN12, (B) HN13, (C) HN30, and (D) CAL27 cell lines. 3 different samples were tested from each cell line (n=2) to study cell to cell variation. Number of cells was estimated from β-Tub concentration per single cell, marked as no cell or single cell on the graph for DSG3. VEGF-C is secreted into the cell culture media in unwashed cell samples, therefore detected with high expression level compared to DSG3, both in the cell and the culture media, marked as Cell+Media on the graph. Estimated biomarker concentration from washed single or no cell samples after online cell lysis for (E) HN12, (F) HN13, (G) HN30, and (H) CAL27 cell lines. 3 different samples were tested from each cell line (n=2) to study cell to cell variation. Number of cells in each sample was estimated using the found β-Tub concentration per single cell, marked as no cell or single

cell on the graph for DSG3 and VEGF-A in the washed cell samples, without the cell culture media, VEGF-A was detected at similar expression level to DGS3.